Chemical Speciation of the Uranyl Ion under Highly Alkaline Conditions. Synthesis, Structures, and Oxo Ligand Exchange Dynamics

David L. Clark,*,[1a] Steven D. Conradson,[1b] Robert J. Donohoe,[1c] D. Webster Keogh,[1d] David E. Morris,[1c] Phillip D. Palmer,[1d] Robin D. Rogers,[1e] and C. Drew Tait[1d]

Chemical Science and Technology Division, Nuclear Materials Technology Division, Materials Science and Technology Division, and the G. T. Seaborg Institute for Transactinium Science, Los Alamos National Laboratory, Los Alamos, New Mexico 87545, and Department of Chemistry, The University of Alabama, Tuscaloosa, Alabama 35487

Received September 22, 1998

The tetramethylammonium counterion was used to suppress formation of insoluble uranate salts, $M_2U_2O_7$, and allow for a detailed structural and spectroscopic characterization of $UO_2(OH)_n^{2-n}$ ($n = 4, 5$) under highly alkaline aqueous solution conditions. Single crystals of $[Co(NH_3)_6]_2[UO_2(OH)_4]_3 \cdot H_2O$ were obtained by cooling a dilute solution of $Co(NH_3)_6Cl_3$ and $UO_2(NO_3)_2 \cdot 6H_2O$ in 3.5 M $(Me_4N)OH$ to 5 °C. The asymmetric unit contains three distinct $UO_2(OH)_4^{2-}$ ions, each displaying a pseudo-octahedral coordination geometry with trans oxo ligands. The three independent $UO_2(OH)_4^{2-}$ ions in the unit cell give average U═O and U−OH distances of 1.82(1) and 2.26(2) Å, respectively. EXAFS data on solid $[Co(NH_3)_6]_2[UO_2(OH)_4]_3 \cdot H_2O$ and aqueous UO_2^{2+} in 3.5 M (Me_4N)-OH solution were collected at the U L_{III} edge, and the resulting radial distribution function shows a single asymmetric peak. For the solid and solution, curve fitting reveals two near neighbors. For the crystalline solid, the first shell was fit with two O atoms at a distance of 1.81(1) Å, and the second shell was fit with 3.9(5) O atoms at a distance of 2.21(1) Å. For the solution sample, the first shell contains two O atoms with a U═O distance of 1.79(1) Å, and the second O shell was fit with 5.2(5) O atoms at a U−O distance of 2.22(1) Å. The bond distances for both the solution and solid state samples correspond relatively well with the single-crystal diffraction data; however, the second-shell coordination number is larger in solution than in the solid state, indicating a greater number of OH ligands in solution than in the solid state. Both EXAFS and X-ray diffraction analyses reveal relatively long axial U═O and short equatorial U−OH bonds. Raman spectra of single crystals of $[Co(NH_3)_6]_2[UO_2(OH)_4]_3 \cdot H_2O$ reveal a symmetrical O═U═O stretch at 796 cm^{-1}, 74 cm^{-1} lower than that for the uranyl aquo ion. In solution, the symmetrical O═U═O stretch is at 786 cm^{-1}, 10 cm^{-1} lower than observed in the solid state. ^{18}O enrichment produces a shift to 752 cm^{-1} confirming the assignment in solution. Luminescence spectroscopy recorded as a function of hydroxide ion concentration reveals that an equilibrium exists between two species, assigned to $UO_2(OH)_4^{2-}$ and $UO_2(OH)_5^{3-}$. The vibronic structure of the luminescence bands was used to determine a vibrational energy of 790 cm^{-1} for $UO_2(OH)_5^{3-}$ to confirm its assignment. ^{17}O NMR and $^{16}O/^{18}O$ Raman spectroscopies also reveal an unprecedented facile ligand exchange between U═O and bulk solvent oxygen atoms. Line-broadening analysis of the ^{17}O NMR data provide activation parameters of $\Delta H^{\ddagger} = 9.8 \pm 0.4$ kcal/mol, $\Delta S^{\ddagger} = -18 \pm 6$ cal/mol·K, and $k_{ex}^{298K} = 45 \pm 15$ s^{-1}. Crystal data for $[Co(NH_3)_6]_2[UO_2(OH)_4]_3 \cdot H_2O$: monoclinic space group $C2/c$, $a = 17.4130(4)$ Å, $b = 12.1794(3)$ Å, $c = 15.3721(4)$ Å, $\beta = 120.384(1)°$, $Z = 4$, R1 = 0.0313, wR2 = 0.0734.

Introduction

The aqueous chemistry of the uranyl(VI) ion (UO_2^{2+}) under acidic conditions is relatively well-known,[2] and uranyl chemistry in near-neutral solutions has received considerable attention due to its importance in radioactive waste isolation and disposal.[3,4] In contrast, aqueous solution chemistry of the uranyl ion under strongly alkaline conditions, such as those found in aging waste tanks within the DOE complex, is only poorly understood.

The hydrolysis reactions of dioxouranium(VI), which begin at pH = 3, have been the subject of extensive study, and an excellent discussion of the species present and their associated thermodynamic data has been reviewed.[5,6] At near-neutral pH values, the uranyl ion forms a number of polymeric U(VI) hydroxide species as outlined in eq 1.

$$m{UO_2}^{2+} + nH_2O \rightleftharpoons (UO_2)_m(OH)_n^{2m-n} + nH^+ \qquad (1)$$

The number and identity of chemical species present in solution vary with the concentration of both UO_2^{2+} (aq) and OH^- (aq). The most prevalent species are monomeric, dimeric,

(1) (a) LANL Mail Stop E500. (b) LANL Mail Stop D429. (c) LANL Mail Stop J586. (d) LANL Mail Stop G739. (e) The University of Alabama.
(2) Katz, J. J.; Seaborg, G. T.; Morss, L. R. *The Chemistry of the Actinide Elements*; Chapman and Hall: London, 1986.
(3) Dozol, M.; Hagemann, R. *Pure Appl. Chem.* **1993**, *65*, 1081.
(4) Clark, D. L.; Hobart, D. E.; Neu, M. P. *Chem. Rev.* **1995**, *95*, 25.
(5) Palmer, D. A.; Nguyen-Trung, C. *J. Solution Chem.* **1995**, *24* (*12*), 1281.
(6) Eliet, V.; Bidoglio, G.; Omenetto, N.; Parma, L.; Grenthe, I. *J. Chem. Soc., Faraday Trans.* **1995**, *91*, 2275.

10.1021/ic981137h CCC: $18.00
Published on Web 03/19/1999

and trimeric ions, with the latter two being favored under higher UO_2^{2+} concentrations ($>10^{-4}$ M). Examples of the most important species include $UO_2(OH)^+$, $(UO_2)_2(OH)_2^{2+}$, $(UO_2)_3(OH)_4^{2+}$, $(UO_2)_3(OH)_5^+$, $(UO_2)_3(OH)_7^-$, $(UO_2)_3(OH)_8^{2-}$, $(UO_2)_3(OH)_{10}^{4-}$, and $(UO_2)_4(OH)_7^+$.[5-7] Solid state structures of uranyl hydroxide complexes are limited, but do include the important cations of formula $(UO_2)_2(\mu\text{-}OH)_2(OH_2)_6^{2+}$ (**I**)[8] and $(UO_2)_3(\mu_3\text{-}O)(\mu_2\text{-}OH)_3(OH_2)_6^+$ (**II**).[9] Both **I** and **II** maintain a pentagonal bipyramidal local coordination geometry about the uranium center, which is also seen in the aquo ion, $UO_2(H_2O)_5^{2+}$ (**III**).[10] These solid state structures are important in understanding the aqueous speciation of the uranyl ion and raise some important questions regarding the true identities of the polymeric ions noted above. For example, the two trimeric species $(UO_2)_3(OH)_5^+$ and $(UO_2)_3(\mu_3\text{-}O)(OH)_3^+$ would be indistinguishable via potentiometric titration experiments since both result in the loss of five protons (eq 1).

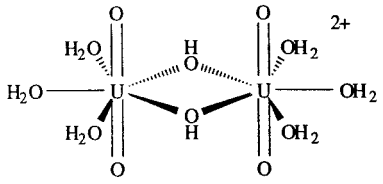

I

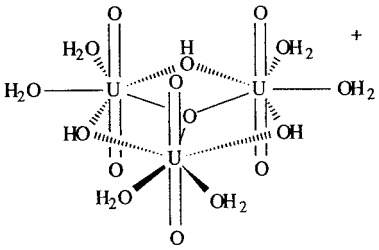

II

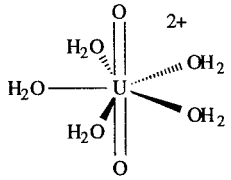

III

With higher OH^- concentrations, some authors have invoked the formation of monomeric $UO_2(OH)_3^-$ to explain their solubility data, but there are no conclusive data to support the existence of either $UO_2(OH)_3^-$ or $UO_2(OH)_4^{2-}$.[7] This is due in part to the fact that, under highly alkaline conditions, uranium will precipitate in the form of a uranate salt, a process used industrially for precipitation of uranium from ore-leach solutions to form $M_2U_2O_7$ ($M = NH_4^+$, Na^+).[2,11] In the present study we employ the tetramethylammonium countercation (as reported by Palmer and Nguyen-Trung)[5] to prevent the precipitation of uranate salts, thereby allowing for the study of uranyl hydroxide complexes under highly alkaline solution conditions.

Results and Discussion

Synthesis and Physicochemical Properties. The study of uranyl hydroxide complexes in alkaline solution poses unique experimental challenges due to the formation of highly insoluble alkali metal mono- and polyuranate salts such as M_2UO_4, $M_2U_2O_7$, etc., where M = Li, Na, K, Cs, or NH_4.[2] Increasing the OH^- concentration of MOH from 3.5 to 15 M had no effect in redissolving uranate salts to produce soluble U(VI) hydroxides. However, U(VI) hydroxide solutions with a uranium concentration of approximately 0.1 M were readily obtained using 1.75−4.5 M tetramethylammonium hydroxide, (TMA)OH. Attempts to crystallize the (TMA)OH-soluble uranyl ion using $C(NH_2)_3^+$, $(n\text{-}Bu)_4N^+$, M^+(18-crown-6) (M = Li, Na, K, or Cs), K^+ encapsulated by 2,2,2-crypt, or addition of NH_4(OH) to a uranyl−(TMA)OH solution either produced powdered material or had no effect at all. However, addition of $Co(NH_3)_6^{3+}$ to (TMA)OH solutions resulted in the deposition of tiny orange crystals of formula $[Co(NH_3)_6]_2[UO_2(OH)_4]_3\cdot H_2O$.

Table 1. Summary of Crystallographic Data for $[Co(NH_3)_6]_2[UO_2(OH)_4]_3\cdot H_2O$

empirical formula	$H_{50}N_{12}O_{19}Co_2U_3$
fw	1354.4
cryst syst	monoclinic
space group	*C*2/*c*
cell dimens	
a, Å	17.4130(4)
b, Å	12.1794(3)
c, Å	15.3721(4)
β, deg	120.384(1)
V, Å^3	2812.35(12)
Z (molecules/cell)	4
D_{calc}, g cm^{-3}	3.199
μ, mm^{-1}	18.462
λ(Mo Kα), Å	0.710 73
temp, °C	−100
measd reflcns	8742
unique intensities	3282
obsd reflcns	2860 ($F > 2\sigma(F)$)
R1	0.0313
wR2	0.0734
goodness-of-fit	1.050

Solid State and Solution Molecular Structure. Single-Crystal X-ray Diffraction. Single crystals of $[Co(NH_3)_6]_2[UO_2(OH)_4]_3\cdot H_2O$ were prepared by cooling a dilute solution of $Co(NH_3)_6Cl_3$ (0.01 M) and $UO_2(NO_3)_2\cdot 6H_2O$ (0.012 M) in 3.5 M (TMA)OH to 5 °C. The resulting crystals were very small and yielded weak intensities, necessitating the use of a diffractometer equipped with a CCD area detector. The data collection and crystallographic parameters are summarized in Table 1, and the selected bond lengths and angles are given in Table 2. A thermal ellipsoid drawing of the repeat unit containing the atom-numbering scheme used in the tables is shown in Figure 1. The asymmetric unit contains three distinct $UO_2(OH)_4^{2-}$ ions, each displaying a pseudo-octahedral coordination geometry with two trans oxo ligands and four hydroxide ligands occupying equatorial coordination sites. The three independent $UO_2(OH)_4^{2-}$ ions in the unit cell give an average U═O distance of 1.82(1) Å, with a range from 1.801(6) to 1.835(5) Å. The O═U═O angles are 180° by symmetry. The O═U−OH angle averages 90(3)° with values ranging from 85.4(2)° to 94.6(2)°.

The average U═O distance of 1.82(1) Å is significantly longer than those seen in other uranyl hydroxide complexes and can be compared to 1.776(6), 1.72(2), and 1.71(1) Å seen in $(UO_2)_2(\mu\text{-}OH)_2(NH_2SO_3)_2(H_2O)_4$,[12] $(UO_2)_2(\mu\text{-}OH)_2(H_2O)_6^{2+}$,[8] and $(UO_2)_2(\mu\text{-}OH)_2(NO_3)_4^{2-}$,[13] respectively. All of the oxo ligands of $UO_2(OH)_4^{2-}$ ions have close contacts to O atoms from OH ligands on neighboring uranium units [average O···

(7) Grenthe, I.; Fuger, J.; Konings, R. J. M.; Lemire, R. J.; Muller, A. B.; Nguyen-Trung, C.; Wanner, H. *Chemical Thermodynamics of Uranium*; Elsevier Science B.V.: New York, 1992; Vol. 1.
(8) Navaza, A.; Villain, F.; Charpin, P. *Polyhedron* **1984**, *3*, 143.
(9) Aberg, M. *Acta Chem. Scand., Ser. A* **1978**, *A32*, 101.
(10) Rogers, R. D.; Kurihara, L. K.; Benning, M. M. *J. Inclusion Phenom.* **1987**, *5*, 645.
(11) Rodriguez, A. S.; Lopez, B. E. M.; Fucugauchi, L. A.; Martinez-quiroz, E. *J. Radioanal. Nucl. Chem.* **1994**, *177*, 279.
(12) Toivonen, J.; Laitinen, R. *Acta Crystallogr.* **1984**, *C40*, 7.
(13) Viossat, P. B.; Dung, N.-H.; Soye, E. C. *Acta Crystallogr.* **1983**, *C39*, 573.

Table 2. Selected Bond Distances (Å) and Angles (deg) for $[Co(NH_3)_6]_2[UO_2(OH)_4]_3 \cdot H_2O$[a]

U(1)−O(1)	1.801(6)	U(2)−O(7)	2.229(5)
U(1)−O(2)	1.829(6)	U(2)−O(6)	2.262(5)
U(1)−O(4)	2.261(5)	U(3)−O(8)	1.823(5)
U(1)−O(3)	2.270(4)	U(3)−O(9)	2.249(5)
U(2)−O(5)	1.835(5)	U(3)−O(10)	2.275(5)
Co−N(1)	1.963(6)	Co−N(3)	1.973(5)
Co−N(6)	1.963(5)	Co−N(5)	1.974(6)
Co−N(2)	1.971(5)	Co−N(4)	1.978(5)
O(1)−U(1)−O(2)	180.000	O(5)−U(2)−O(5B)	180.0
O(1)−U(1)−O(4)	91.04(11)	O(5)−U(2)−O(7)	85.4(2)
O(2)−U(1)−O(4)	88.96(10)	O(5)−U(2)−O(7B)	94.6(2)
O(4A)−U(1)−O(4)	177.9(2)	O(7)−U(2)−O(7B)	180.0
O(4)−U(1)−O(3A)	88.1(2)	O(5)−U(2)−O(6)	86.4(2)
O(1)−U(1)−O(3)	88.08(11)	O(5B)−U(2)−O(6)	93.6(2)
O(2)−U(1)−O(3)	91.92(11)	O(7)−U(2)−O(6)	91.4(2)
O(4)−U(1)−O(3)	92.0(2)	O(7B)−U(2)−O(6)	88.6(2)
O(3A)−U(1)−O(3)	176.2(2)	O(6)−U(2)−O(6B)	180.0
O(8)−U(3)−O(8C)	180.0	O(8C)−U(3)−O(10)	92.3(2)
O(8)−U(3)−O(9)	93.4(2)	O(9)−U(3)−O(10)	90.2(2)
O(8C)−U(3)−O(9)	86.6(2)	O(9)−U(3)−O(10C)	89.8(2)
O(9)−U(3)−O(9C)	180.0	O(9C)−U(3)−O(10C)	90.2(2)
O(8)−U(3)−O(10)	87.7(2)	O(10)−U(3)−O(10C)	180.0
N(1)−Co−N(6)	86.2(2)	N(1)−Co−N(4)	91.2(3)
N(1)−Co−N(2)	90.4(2)	N(6)−Co−N(4)	88.8(2)
N(6)−Co−N(2)	88.6(2)	N(2)−Co−N(4)	176.8(2)
N(1)−Co−N(3)	91.3(2)	N(3)−Co−N(4)	91.0(2)
N(6)−Co−N(3)	177.5(2)	N(5)−Co−N(4)	88.2(2)
N(2)−Co−N(3)	91.7(2)	N(2)−Co−N(5)	90.2(2)
N(1)−Co−N(5)	179.2(2)	N(3)−Co−N(5)	89.2(2)
N(6)−Co−N(5)	93.3(2)		

[a] Symmetry transformations used to generate equivalent atoms: A $= -x + 2, y, -z + 3/2$; B $= -x + 2, -y + 2, -z + 1$; C $= -x + 3/2, -y + 3/2, -z + 1$.

O = 2.76(7) Å] or NH_3 ligands from adjacent $Co(NH_3)_6^{3+}$ units [average O···N = 3.2(1) Å]. In addition, some OH ligands have close contacts to the lattice H_2O molecule [average O···O = 2.85(2) Å] or $Co(NH_3)_6^{3+}$ ions [average O···N = 3.1(1) Å]. These distances are well within the range expected for weak H-bonding interactions.[14] The U═O bond distances appear to have some relation to the number of H-bonding interactions. For example, the shortest U═O distance of 1.801(6) Å is seen for U(1)−O(1), and O(1) has only one intermolecular O···N interaction of 3.117(6) Å to a $Co(NH_3)_6^{3+}$ unit. In contrast, the longest U═O distance of 1.835(5) Å is found between U(2) and O(5), and O(5) has close intermolecular contacts with an OH ligand [O(10), 2.735(7) Å] and with amine nitrogen atoms N(2) and N(4) of a $Co(NH_3)_6^{3+}$ unit [3.311(7) and 3.098(8) Å, respectively].

The average terminal U−OH distance is 2.26(2) Å, with values spanning the relatively narrow range 2.229(5)−2.275(5) Å. To the best of our knowledge there are no terminal uranyl hydroxide structures reported for comparison. The only known distances of 2.293(9), 2.36(1), 2.29(1), and 2.372(4) Å are for bridging OH ligands in $(UO_2)_2(\mu\text{-OH})(C_5H_3O_3)_3(H_2O)_2$,[15] $(UO_2)_2(\mu\text{-OH})_2(NO_3)_4^{2-}$,[13] $(UO_2)_2(\mu\text{-OH})_2(H_2O)_6^{2+}$,[8] and $(UO_2)_2(\mu\text{-OH})_2(NH_2SO_3)_2(H_2O)_4$,[12] respectively. As expected, these U−μ-OH distances are slightly longer than the terminal U−OH distances reported here. The terminal U−OH distances are much more typical of the distances found for terminal U−OR bonds in uranyl alkoxide complexes, which generally span 2.15−2.25 Å.[16,17] The average U−OH distance of 2.26(2) Å can be compared to the average terminal U−OR distances of 2.152(5), 2.197(4), and 2.246(4) Å observed in $UO_2(O\text{-}t\text{-}Bu)_2(OPPh_3)_2$,[16] $UO_2(O\text{-}2,6\text{-}i\text{-}Pr_2C_6H_3)_2(py)_3$, and $UO_2(O\text{-}2,6\text{-}Me_2C_6H_3)_4^{2-}$,[17] respectively. It is noteworthy that these uranyl alkoxide complexes not only display short U−OR bonds comparable to the U−OH bonds seen in $UO_2(OH)_4^{2-}$ but also exhibit rather long U═O bond lengths of 1.792(4), 1.789(4), and 1.814(4) Å, respectively. The latter were attributed to U═O···Na interactions in the solid state. The $Co(NH_3)_6^{3+}$ unit is pseudo-octahedral and displays bond lengths and angles in the normal ranges.

XAFS Studies. X-ray absorption fine structure (XAFS) spectroscopy was used to determine structural details (bond distances and coordination numbers) of the uranyl ion in (TMA)OH solution. In addition, with the preponderance of polymeric uranyl hydroxide ions $(UO_2)_m(OH)_n^{2m-n}$ identified in near-neutral solution (eq 1),[5,7] extended XAFS (EXAFS) spectroscopy could be used to differentiate between simple monomeric and polymeric species, which might be expected to exhibit a U−U backscattering interaction in the solution spectrum. We have successfully used such a feature in the identification of the polymeric uranyl carbonato anion $(UO_2)_3(\mu\text{-}CO_3)_3(CO_3)_3^{6-}$ in carbonate solutions.[18]

X-ray absorption measurements on solid $[Co(NH_3)_6]_2[UO_2(OH)_4]_3 \cdot H_2O$ and a solution of UO_2^{2+} in 3.5 M (TMA)OH were performed at the uranium L_{III} edge. The background-subtracted k^3-weighted EXAFS spectrum is shown in Figure 2a, where experimental data are shown as a solid line, and the theoretical fit is indicated as a dashed line. The Fourier transform modulus and theoretical fit (without phase corrections) of the k^3-weighted EXAFS data are shown in Figure 2b. Note that because the FT is not corrected for the EXAFS phase shift, the peak positions are 0.2−0.5 Å lower than the actual U−O distances.[18]

The theoretical EXAFS modeling code, FEFF7,[19,20] of Rehr et al. was employed to calculate the backscattering phases and amplitudes of the individual neighboring atoms, using symmetrical monomeric $UO_2(OH)_n^{2-n}$ model structures, where n varied between 4, 5, and 6 with local tetragonal-, pentagonal-, and hexagonal-bipyramidal coordination environments, respectively. The fitting parameters found for the U solid and solution structures are listed in Table 3, where the data were fit from $k = 3.00-11.70$ Å^{-1}. The values for the bond distances and number of atoms in each shell are consistent with the formation of a monomeric uranyl hydroxide complex quite similar to the species found in the solid state. Evaluations of both the k^3-weighted $\chi(k)$ (Figure 2a) and $\chi(R)$ (Figure 2b) indicate a reasonable fit in both phase and amplitude. Curve fitting reveals that the single asymmetric peak in both FT spectra (Figure 2b) contains two shells with a small bond length separation. Since the coordination number is highly correlated with both the amplitude (S_0^2) and Debye−Waller (σ^2) factors, reliable coordination numbers are best obtained when the data can be compared to a standard of known coordination number. Therefore, we measured single crystals of $[Co(NH_3)_6]_2[UO_2(OH)_4]_3 \cdot H_2O$ by XAFS for comparison with our solution data.

(14) Pauling, L. *The Nature of the Chemical Bond*, 3rd ed.; Cornell University Press: Ithaca, NY, 1960; p 644.
(15) Alcock, N. W.; Kemp, T. J.; Leciejewicz, J. *Inorg. Chim. Acta* **1991**, *184*, 203.
(16) Burns, C. J.; Smith, D. C.; Sattelberger, A. P.; Gray, H. B. *Inorg. Chem.* **1992**, *31*, 3724.
(17) Barnhart, D. M.; Burns, C. J.; Sauer, N. N.; Watkin, J. G. *Inorg. Chem.* **1995**, *34*, 4079.
(18) Allen, P. G.; Bucher, J. J.; Clark, D. L.; Edelstein, N. M.; Ekberg, S. A.; Gohdes, J. W.; Hudson, E. A.; Kaltsoyannis, N.; Lukens, W. W.; Neu, M. P.; Palmer, P. D.; Reich, T.; Shuh, D. K.; Tait, C. D.; Zwick, B. D. *Inorg. Chem.* **1995**, *34*, 4797.
(19) Ankudinov, A. L.; Rehr, J. J. *Phys. Rev. B* **1997**, *56*, R1712.
(20) Ankudinov, A. L. Ph.D. Thesis, University of Washington, 1996.

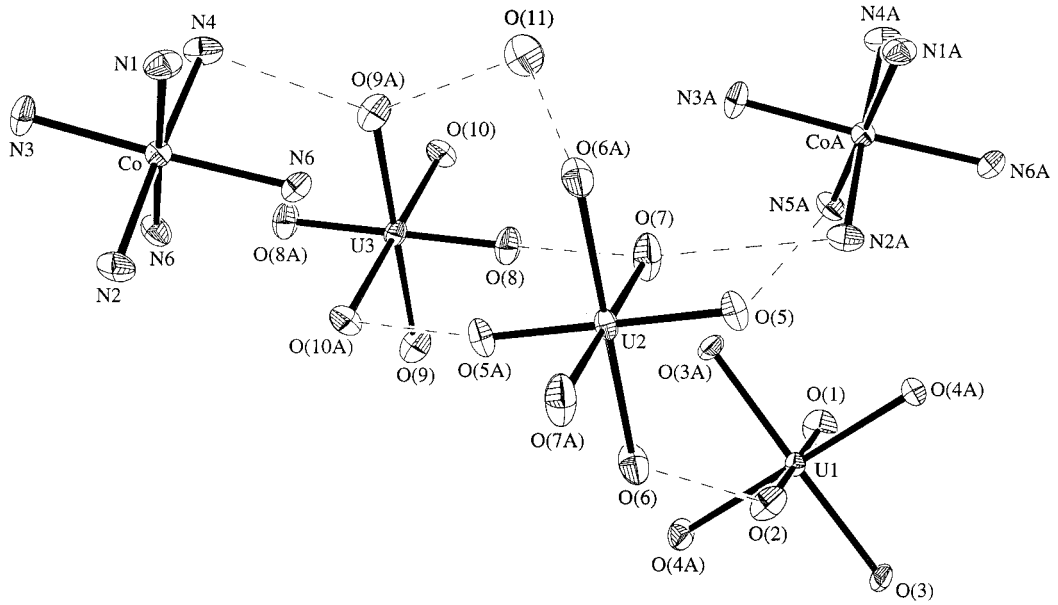

Figure 1. Thermal ellipsoid drawing of the repeat unit of $[Co(NH_3)_6]_2[UO_2(OH)_4)]_3 \cdot H_2O$ showing the atom-labeling scheme used in the tables.

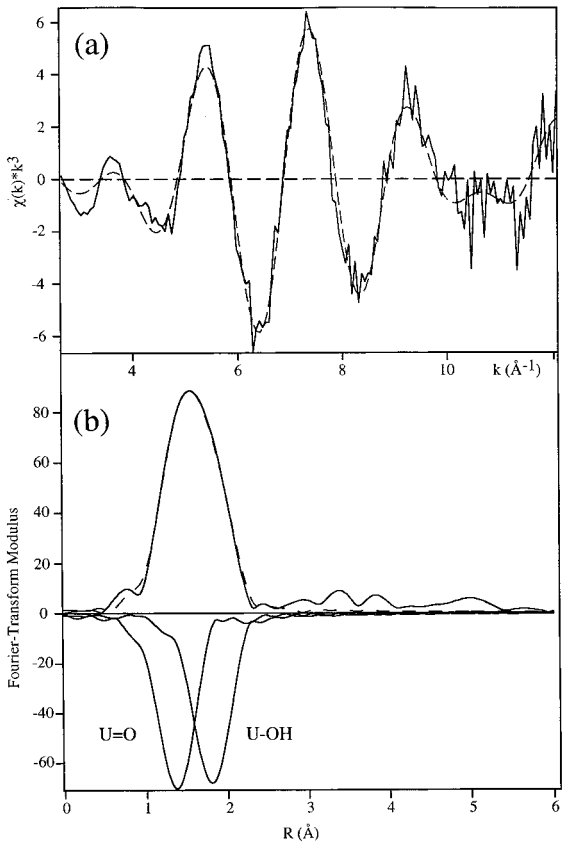

Figure 2. (a) Background-subtracted k^3-weighted EXAFS spectra (solid line) and fit (dashed line) of U(VI) in 3.5 M (TMA)OH solution. (b) Fourier tranform without phase corrections of the k^3-weighted EXAFS spectra of U(VI) in 3.5 M (TMA)OH solution ($R = 0-6$ Å). The solid line is the experimental data, and the dashed line is the theoretical fit. Shown with negative FT amplitudes are the single shell contributions to the fit.

The background-subtracted k^3-weighted $\chi(k)$ and $\chi(R)$ of the single-crystal sample are very similar to those of the solution spectra and are therefore not shown here. The EXAFS structural data and fit parameters for the single-crystal data are summarized in Table 3, where they can be compared to the solution results. The first shell was fit with two O atoms with a U═O distance of 1.81(1) Å, and the second shell was best fit with a nominal 3.9 O atoms at a U−O distance of 2.21(1) Å. The distance and coordination numbers compare well with the X-ray diffraction data, which gave U═O and U−OH distances of 1.82(1) and 2.26(1) Å, respectively. For the solution data the first shell was fit with two O atoms with a U═O distance of 1.79(1) Å, and the second shell was best fit with 5.2 O atoms at a U−O distance of 2.22(1) Å. The best fits of the EXAFS data on the solid and solution samples clearly indicates a larger number of OH^- ligands in solution ($n = 5$) compared to the value ($n = 4$) found in the solid state.

Table 3. Summary of EXAFS Results for U(VI) in 3.5 M (TMA)OH Solution and $[Co(NH_3)_6]_2[UO_2(OH)_4]_3 \cdot H_2O$ Solid Fitted to k^3 [a]

shell	n	r, Å	σ^2(Å^2)	ΔE_0
Solid $[UO_2(OH)_4]_3[Co(NH_3)_6]_2 \cdot H_2O$				
U═O	2.0[b]	1.81(1)	0.0020(13)	8.7
U−OH	3.9(5)	2.21(1)	0.0043(1)	4.3
U═O, ms		3.54(1)	0.0006	3.4
Solution $[UO_2(OH)_5]^{3-}$				
U═O	2.0[b]	1.79(1)	0.0017(4)	3.2
U−OH	5.3(5)	2.22(1)	0.0037(8)	1.6
U═O, ms		3.63(1)	0.0119(57)	5.7

[a] $k = 3.00-11.7$, $S_0^2 = 0.8$, ms = multiple scattering. [b] Fixed at this value.

A structural model for a uranyl ion with five OH ligands in solution is chemically reasonable, especially in light of the preponderance of uranium(VI) complexes which exhibit an equatorial coordination number of 5 (i.e., **I**, **II**, and **III**) for monodentate ligands.[8-10] Thus these data are consistent with $UO_2(OH)_4^{2-}$ (**IV**) in the solid state and $UO_2(OH)_5^{3-}$ (**V**) in 3.5 M (TMA)OH solution.

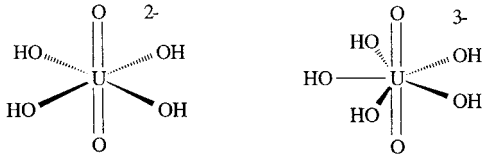

IV **V**

During the past several years, a number of EXAFS studies

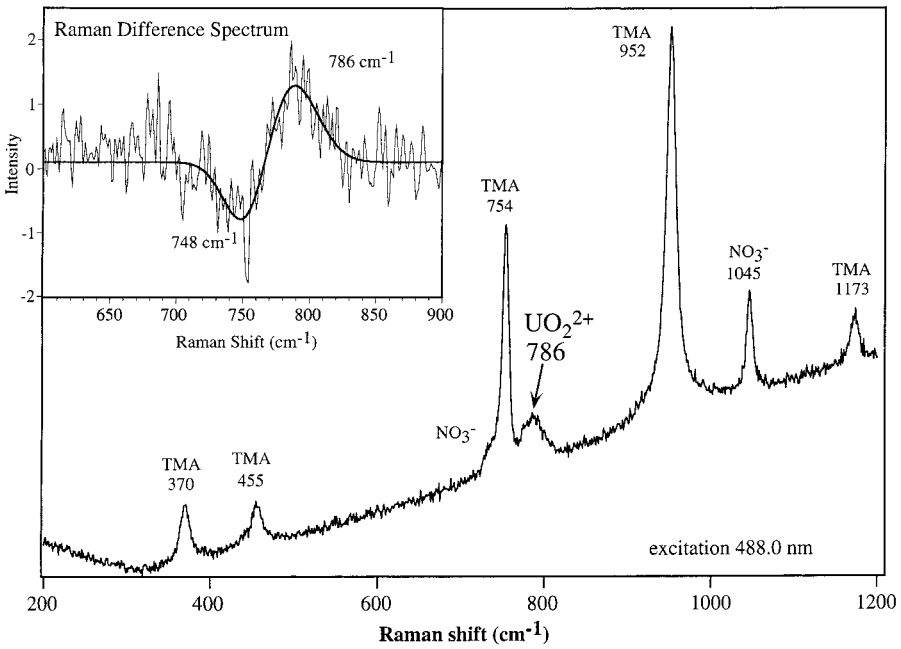

Figure 3. Raman spectrum of 0.1 M UO_2^{2+} in 3.5 M (TMA)OH. The rising background to higher frequency is due to uranyl luminescence. The inset shows a difference plot of the ^{18}O- and ^{16}O-labeled Raman spectra clearly indicating the presence of the two different vibrational bands.

of uranyl ions have been reported,[18,21−23] where the data analyses required the inclusion of a multiple scattering pathway with an effective R value twice that of the uranyl U═O distance. In $UO_2(CO_3)_3^{4-}$, for example, this path was calculated to have an amplitude ca. 21% of the single uranyl scattering path.[18] A similar multiple scattering pathway improves the fit for both the solid and solution data, despite the lengthened U═O bond. No evidence of a U- -U backscattering interaction expected for a polymeric species was found, consistent with maintenance of a monomeric species both in the solid state and in solution.

The observation of a higher equatorial coordination number in solution than in the solid state is suggestive that an equilibrium could exist between $UO_2(OH)_4^{2-}$ (**IV**) and $UO_2(OH)_5^{3-}$ (**V**) ions. While these data are certainly consistent with a greater equatorial coordination number for uranyl in (TMA)OH solution than in the solid state, the very short time scale of XAFS renders it unsuitable for determination of equilibria. Therefore, other spectroscopic techniques were chosen to examine whether an equilibrium of the type outlined in eq 2 could be taking place in solution.

$$UO_2(OH)_4^{2-} + OH^- \rightleftharpoons UO_2(OH)_5^{3-} \qquad (2)$$

Spectroscopic Studies. Vibrational Spectroscopy. Our structural studies revealed a lengthening and presumably weakening of the U═O bond for the uranyl ion in 3.5 M (TMA)OH solution, relative to the aquo ion, $UO_2(H_2O)_5^{2+}$. The Raman shift of the symmetrical ν_1 O═U═O stretch is a much more sensitive probe of bond strength than bond length, with stronger bonds having higher vibrational frequencies.[18,24,25] Uranyl bond strength differences between compounds have traditionally been attributed to the strength of metal−ligand bonding in the equatorial plane.[26] Specifically, ligand-to-metal σ- and π-bonding of the equatorial ligands increases the electron density on the uranium metal center and increases electrostatic repulsion with the highly negative axial oxygen atoms to weaken the U═O bonds.

A Raman spectroscopic analysis was performed on single crystals of $[Co(NH_3)_6]_2[UO_2(OH)_4]_3 \cdot H_2O$ and UO_2^{2+} in 3.5 M (TMA)OH solution to probe the symmetrical ν_1 O═U═O stretch in both systems. If there is a difference in the number of equatorial OH^- ligands between the solid state and solution species, this could manifest itself as a difference in the ν_1 stretch in these states. The Raman spectrum of single crystals of $[Co(NH_3)_6]_2[UO_2(OH)_4]_3 \cdot H_2O$, where it is known definitively that $n = 4$, reveals a O═U═O ν_1 frequency at 796 cm^{-1}. The Raman spectra (Figure 3) of the uranyl solutions reveal a band at 786 cm^{-1} (10 cm^{-1} lower in energy than the solid). To the best of our knowledge, this vibrational frequency represents the lowest Raman shift ever reported for a U(VI) complex.[27] The other bands observed in the Raman spectrum (Figure 3) have been positively assigned to Me_4N^+ and NO_3^- ions by repeating the experiment with a control solution consisting of 3.5 M (TMA)OH and 0.1 M NO_3^-. If a Cl^- counterion is used in the alkaline solution preparation, the Raman spectrum shows a slight shift in the O═U═O ν_1 to 784 cm^{-1}. The difference in these two Raman values could be due to solid state effects such as crystal packing and hydrogen bonding or could be indicative of a larger number of hydroxo ligands present in solution.

This sensitivity of the ν_1 Raman mode to the number of equatorial ligands complexed to the uranyl ion is well-known. Nguyen-Trung et al.[27] reported a linear correlation between the coordination number of the equatorial ligand and the Raman shift as outlined in eq 3. In eq 3, 870 is the observed Raman shift (in cm^{-1}) for $UO_2(H_2O)_5^{2+}$ ($n = 0$, triflic acid solution) ion, A is a coefficient characteristic of a given ligand (CO_3^{2-},

(21) Allen, P. G.; Shuh, D. K.; Bucher, J. J.; Edelstein, N. M.; Reich, T.; Denecke, M. A.; Nitsche, H. *Inorg. Chem.* **1996**, *35*, 784.
(22) Hudson, E. A.; Allen, P. G.; Terminello, L. J.; Denecke, M. A.; Reich, T. *Phys. Rev. B: Condens. Matter* **1996**, *54*, 156.
(23) Reich, T.; Moll, H.; Denecke, M. A.; Geipel, G.; Bernhard, G.; Nitsche, H.; Allen, P. G.; Bucher, J. J.; Kaltsoyannis, N.; Edelstein, N. M.; Shuh, D. K. *Radiochim. Acta* **1996**, *74*, 219.
(24) Jones, L. H. *Spectrochim. Acta* **1959**, *11*, 409.
(25) Jones, L. H. *Spectrochim. Acta* **1958**, *10*, 395.
(26) McGlynn, S. P.; Smith, J. K.; Neely, W. C. *J. Chem. Phys.* **1961**, *35*, 105.
(27) Nguyen-Trung, C.; Begun, G. M.; Palmer, D. A. *Inorg. Chem.* **1992**, *31*, 5280.

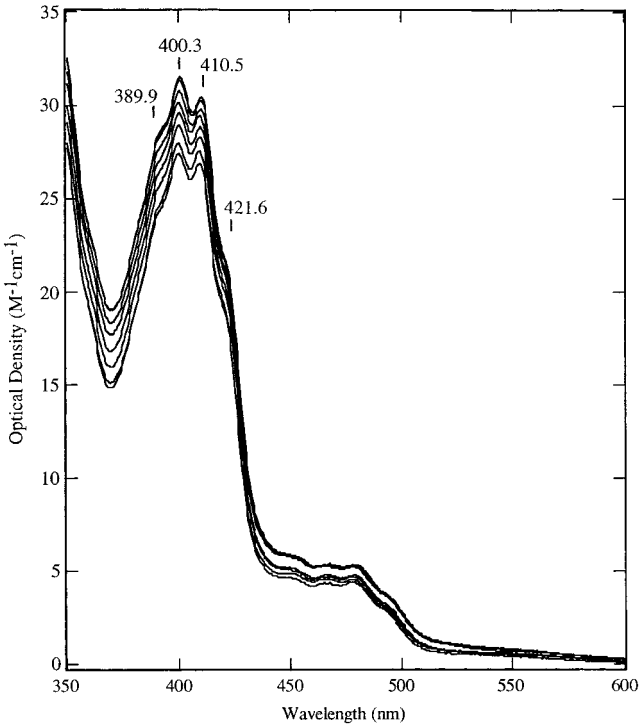

Figure 4. Room-temperature UV−visible electronic absorption spectra for 4.75 mM UO_2^{2+} in aqueous (TMA)OH solution. [(TMA)OH] conentrations are 2.51 M (most intense spectrum), 2.23 M, 2.01 M, 1.81 M, 1.54 M, 1.33 M, 1.09 M, and 0.86 M (least intense spectrum). Absorption maxima (nm) are indicated for four prominent vibronic features.

Cl^-, OH^-, etc.), and n is the average coordination number for the equatorial ligand. We therefore anticipated that Raman

$$\nu_1\ (\mathrm{cm}^{-1}) = 870 - An \qquad (3)$$

spectroscopy could help establish the number of equatorial OH^- ligands in solution. In the case of OH^- ligands, the characteristic coefficient A was determined to be 21.5 ± 1.0 cm^{-1} by study of $(UO_2)_m(OH)_n^{2m-n}$ hydrolysis products.[27] However, we have only observed a 10 cm^{-1} shift between solid state (796 cm^{-1}, $n = 4$) and solution (786 cm^{-1}, $n = 5$) for our monomeric species. Using the relationship in eq 3, one would predict vibrational frequencies for $UO_2(OH)_n^{2-n}$ of 784 cm^{-1} ($n = 4$) and 762 ($n = 5$). As a result, we do not believe that the vibrational correlation observed in the hydrolysis polymers can be applied to the monomeric species observed under these highly alkaline conditions of our study.

Electronic Absorption and Emission Spectroscopy. The visible electronic absorption spectra of UO_2^{2+} in 2.51−0.86 M (TMA)OH are shown in Figure 4. The main absorption feature is a fine-structured band with $\lambda_{max} = 400$ nm ($\epsilon = 32$ M^{-1} cm^{-1}). This feature is slightly blue-shifted when compared to the UO_2^{2+} aquo ion in 1 M $HClO_4$ ($\lambda_{max} = 409$ nm, $\epsilon = 8$ M^{-1} cm^{-1}) and consists of four resolved vibronic lines (Figure 4). The average line separation for the U(VI) hydroxide complex is 643 cm^{-1}, compared to 706 cm^{-1} for the aquo ion. The smaller energetic splitting in the hydroxide complex suggests a weaker excited state U═O bond relative to the uranyl aquo ion and is consistent with the U═O bond lengthening and weakening seen in structural (XRD and XAFS) and vibrational (Raman) studies of the ground state complex.

The room-temperature UV−visible electronic absorption spectral data for UO_2^{2+} as a function of (TMA)OH concentration

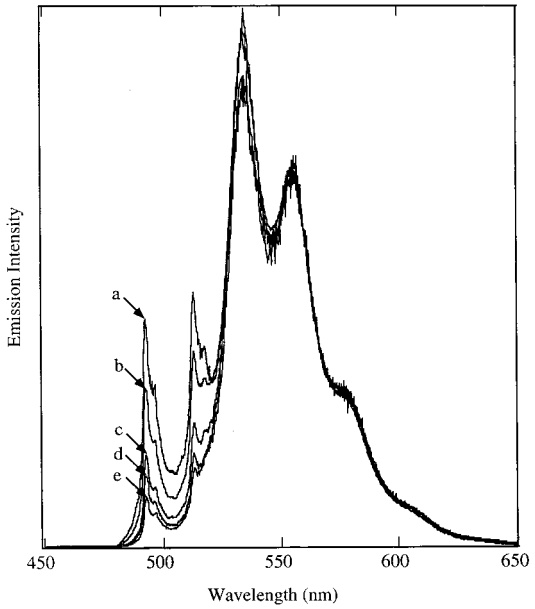

Figure 5. Liquid-nitrogen temperature emission spectra obtained with 400 nm CW excitation for 4.75 mM UO_2^{2+} in aqueous (TMA)OH solution. Spectral intensities have been normalized to the peak intensity at 555 nm to facilitate comparison. [(TMA)OH] concentrations are 2.51 M (a), 2.23 M (b), 2.01 M (c), 1.81 M (d), and 0.86 M (e). These spectra show the increase in intensity of emission features at 493 and 513 nm with increasing OH^- concentration, indicating an equlibrium between uranyl hydoxide species.

(Figure 4) show a slight, monotonic increase in absorbance with increasing (TMA)OH concentration. The increase is most pronounced [change in optical density, $\Delta OD = 4$ M^{-1} cm^{-1} from 0.75 to 2.5 M (TMA)OH] in the region of the more intense vibronically resolved bands (ca. 385−425 nm). In addition, there is a small but smooth shift to longer wavelength in these more intense vibronic bands with increasing (TMA)OH concentration. For the vibronic band at approximately 410 nm, this shift is ca. 0.75 nm (50 cm^{-1}) from 0.75 to 2.5 M (TMA)OH. This behavior could be indicative of a change in speciation. However, there is no evidence in these absorption spectra for isosbestic points. The lowest OH^- concentration studied was 0.05 M, where the absorption spectrum was consistent with that reported previously for a mixture of polymeric $(UO_2)_m(OH)_n^{2m-n}$ species ($\lambda_{max} =$ 420 nm, $\epsilon = 43$ M^{-1} cm^{-1}).[28]

The room-temperature luminescence data for UO_2^{2+} in (TMA)OH solution show only weak, broad, and poorly structured emission bands over a broad range of (TMA)OH concentrations. For comparison, the fully aquated uranyl monomer $[UO_2(OH_2)_5^{2+}]$ in solution at pH 1−2 has a vibronically well resolved, albeit weak, emission spectrum even at room temperature.[29]

In contrast, the continuous wave (CW) emission data for UO_2^{2+} in (TMA)OH solution at liquid nitrogen temperature reveal very intense, structured vibronic bands (Figure 5). These emission data clearly show evidence for *two distinct emissive species*; one (hereafter referred to as species A) with prominent vibronic bands at 493 and 513 nm and the other (species B) with prominent vibronic bands at lower energy (535, 555, and 577 nm) indicating a probable equilibrium. The spectral features characteristic of species A increase in intensity relative to those

(28) Meinrath, G.; Kato, Y.; Yoshida, Z. *J. Radioanal. Nucl. Chem.* **1993**, *174*, 299.
(29) Morris, D. E.; Chisholm-Brause, C. J.; Barr, M. E.; Conradson, S. D.; Eller, P. G. *Geochim. Cosmochim. Acta* **1994**, *58*, 3613.

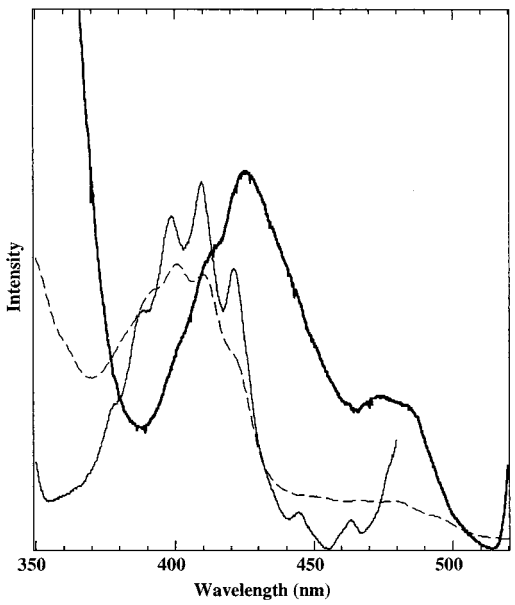

Figure 6. Comparison of liquid-nitrogen temperature CW excitation spectra and room-temperature absorption spectrum for 4.75 mM UO_2^{2+} in 2.51 M aqueous (TMA)OH solution. Heavy line: excitation spectrum obtained at 540 nm. Thin line: excitation spectrum obtained at 500 nm. Dashed line: absorption spectrum. Intensities are arbitrary and have been manipulated to facilitate comparison.

of species B with increasing (TMA)OH concentration, indicating that the concentration of species A increases with increasing (TMA)OH concentration. However, in the absence of detailed photophysical data (e.g., molar absorptivities and luminescence quantum yields for the individual species) it is not possible at this time to translate these emission intensity data into either absolute concentrations or relative concentration ratios for the two species.

The liquid-nitrogen temperature CW excitation spectra (Figure 6) provide additional compelling evidence for the existence of two species in equilibrium in these solutions. Specifically, the excitation spectrum obtained while monitoring emission in the highest energy vibronic band of species A (500 nm) is very distinct from that obtained while monitoring emission within the vibronic manifold of species B (540 nm). Furthermore, the solution UV−visible absorption spectrum (overlaid in Figure 6 for comparison) is in excellent agreement with the excitation spectrum associated with species A. (Notably, this good correlation also indicates that the temperature change from room temperature to liquid nitrogen does not totally perturb the solution speciation in these samples, although the extent to which the temperature change affects the equilibrium concentrations of the species is unknown.) The agreement between the UV−visible spectrum and the excitation spectrum obtained at 500 nm suggests that the dominant contribution to the absorption spectrum comes from species A over the entire (TMA)OH concentration range employed for these studies. In fact, the slight increase in absorbance in the UV−visible spectra occurs principally over a wavelength range (~385 to 425 nm) in which the excitation spectrum for species B shows a local minimum in intensity. Thus, the observed increase in absorbance seems most likely attributable to an increase in the solution concentration of species A. While it is possible that there is a large difference in the molar absorptivity of species A versus species B, the absorption data most likely demonstrate that the concentration of species A exceeds that of species B by a substantial amount.

This conclusion may seem at odds with the relative emission intensity data of species A and B shown in Figure 5. However, emission intensities are determined by a complex interplay of numerous factors including concentration, absorption cross section, and excited state radiative and nonradiative decay rates and mechanisms. The experimental excited state decay rates can, in general, provide some insight into these photophysical parameters. In particular, in the absence of photochemical deactivation processes (likely here since there are no good substrates with which the excited UO_2^{2+} can react via redox mechanisms), the measured decay rate reflects the contributions from radiative and nonradiative (principally electronic to vibrational energy transfer) rates.[30] In the present case, however, there is very little difference in the measured decay rates at liquid nitrogen temperature for species A ($\tau_{meas} = 220 \pm 6$ μs determined at 492.5 nm for five samples) versus that for species B ($\tau_{meas} = 191 \pm 6$ μs determined at 534 nm for five samples). Not surprisingly given this agreement between decay rates, all decay curves were satisfactorily fit with a single-exponential term, even though the decay data at 534 nm should contain some contribution from emission by species A as well as species B. Since the radiative decay rate constant appears in the pre-exponential term for the time-dependent emission intensity,[30] it is likely that a difference in this parameter between species A and B is principally responsible for the observed difference in the emission intensities in Figure 5.

The vibronic structure observed in the emission and excitation or absorption spectra is due principally to the totally symmetric stretching vibration of the UO_2^{2+} moiety in the ground electronic state (emission spectra) or the excited electronic state(s) (excitation and absorption). For the emission spectral data shown in Figure 5, the spectra were fit using standard nonlinear least-squares methods and either Gaussian or Voigt fitting functions to determine accurately the positions of the vibronic peaks. The vibronic structure seen in the emission spectral bands attributed to species A actually appears to have contributions from two vibrational modes. However, the primary progression (established by the bands at 493 and 513 nm) was determined to have a vibrational energy of 790 cm^{-1}. The sole progression seen in the spectrum attributed to species B and defined by the bands at 535, 555, and 577 nm was determined to have an energy spacing of 720 cm^{-1}. However, the breadth of the vibronic bands in the spectrum of species B (Figure 5) is much greater than that in the spectrum of species A. This could be an indication of a MIME effect (i.e., convolution of vibronic progressions in two or more normal modes)[31,32] in the spectrum of species B that would make any direct correlation between observed vibronic spacing and the energy of the totally symmetric uranyl stretching mode unreliable. Notably, a single totally symmetric uranyl stretching mode for UO_2^{2+} in 2.5 M (TMA)OH at room temperature was observed by Raman spectroscopy with an energy of 786 cm^{-1}, in excellent agreement with the value determined from the emission data for species A. Thus we can reasonably assign species A to $UO_2(OH)_5^{3-}$

(30) More precisely, for the integrated emission intensity obtained from CW excitation experiments, it is the luminescence quantum yield (Φ_{em}) that appears in the intensity expression. However, in the absence of photochemical processes, $\Phi_{em} = [k_r/(k_r + k_{nr})]$ where k_r and k_{nr} are the radiative and nonradiative rate constants, respectively, and the denominator is related to the measured emission decay rate constant ($\tau_{meas} = 1/(k_r + k_{nr})$). Since measured decay rates are comparable for both species A and B (see text), comparisons of quantum yields from the CW data are essentially the same as comparisons of the radiative rate constants for the two species.

(31) Tutt, L.; Tannord, D.; Heller, E. J.; Zink, J. I. *Inorg. Chem.* **1982**, *21*, 3858.
(32) Tutt, L. W.; Zink, J. I.; Heller, E. J. *Inorg. Chem.* **1987**, *26*, 2158.

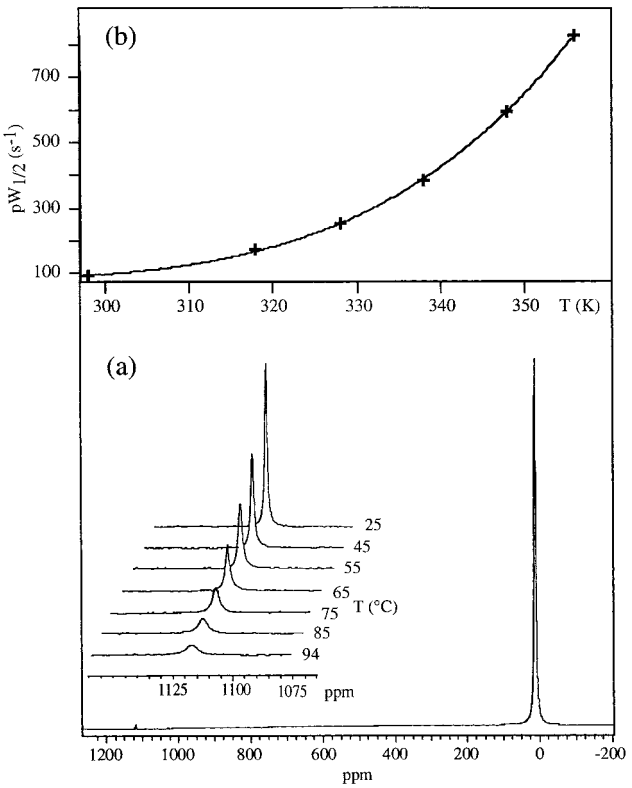

Figure 7. (a) Uranyl region (inset) of the variable-temperature ^{17}O NMR spectra (67.8 MHz) of UO_2^{2+} in 3.5 M (TMA)OH. (b) Kinetic analysis of the ^{17}O NMR line-width data for UO_2^{2+} in 3.5 M (TMA)-OH.

and species B to $UO_2(OH)_4^{2-}$ in the equilibrium outlined in eq 2. The absence of a second totally symmetric uranyl stretching mode attributable to $UO_2(OH)_4^{2-}$ in the solution Raman spectrum is a consequence of the apparent low concentration of this species in the room-temperature solution as noted above.

^{17}O NMR Spectroscopy. The absorption and emission data indicated the presence of at least two different uranium-containing species in solution. To directly probe this possibility, ^{17}O NMR was utilized. The well-known chemical inertness[33] of the oxo ligands in uranyl(VI) compounds makes ^{17}O NMR spectroscopy an extremely useful spectroscopic probe of uranyl complexes in solution.[18,34] ^{17}O-Enriched samples of uranyl ions were prepared electrochemically in 1 M $HClO_4$ as described elsewhere.[18] The ^{17}O NMR spectrum (67.8 MHz) of a 0.1 M solution of 4% ^{17}O-enriched UO_2^{2+} in 3.5 M (TMA)OH and 20% ^{17}O-enriched H_2O revealed two resonance lines as shown in Figure 7a. A singlet at $\delta = 1117$ ppm ($\Delta\nu_{1/2} = 29.5$ Hz) is assigned to the uranyl oxygen atoms, and the singlet at $\delta = 10$ ppm is assigned to the chemical shift weighted average of bulk H_2O, and free and bound OH^- involved in rapid chemical exchange. The chemical shift for the uranyl oxygen atom can be compared to $UO_2(OH_2)_5^{2+}$ in 1 M $HClO_4$ ($\delta = 1121$ ppm, $\Delta\nu_{1/2} = 9$ Hz), and $UO_2(CO_3)_3^{4-}$ ($\delta = 1098$ ppm, $\Delta\nu_{1/2} = 6$ Hz).[18]

Ligand Exchange Phenomena. During preliminary ^{17}O NMR experiments, 4% ^{17}O-enriched UO_2^{2+} (aq) was dissolved in 3.5 M (TMA)OH solutions. Remarkably, the ^{17}O NMR spectra of these solutions showed either no oxo resonance or only a very weak signal due to uranyl oxygen atoms. This was highly unusual in light of the ease of observation of the uranyl oxygen resonance in our laboratories under similar enrichment and concentrations for uranyl systems containing aquo or carbonato ligands.[18] The use of a more highly enriched system (20% ^{17}O) ultimately led to the observation of a uranyl resonance at $\delta = 1117$ ppm ($\Delta\nu_{1/2} = 29.5$ Hz) in 3.5 M (TMA)-OH. These data suggested that chemical exchange of oxo ligands might be responsible for a deincorporation of the ^{17}O-spin label in enriched samples. For the uranyl(VI) ion, the chemical inertness of oxo ligands is well-known, and the half-life for room-temperature oxo ligand exchange under acidic conditions has been estimated by Gordon and Taube to be 40 000 h.[33] Uranyl oxo ligand exchange has only been accomplished under acidic conditions with highly energetic techniques such as photolysis, which operates via photoreduction to transient uranyl(V), UO_2^+.[35−38] While unprecedented for the uranyl(VI) ion, oxo ligand exchange processes have been reported in alkaline solution for transition metal complexes such as MO_4^{2-} (M = Mo, W)[39] and $MO_2(CN)_4^{n-}$ [M = Mo(IV), W(IV), $n = 4$; Tc(V), Re(V), $n = 3$][40,41] and for Np(VII).[42]

Oxo ligand exchange with the solvent was confirmed via variable temperature line-width analysis of the uranyl ^{17}O resonance. For comparison, UO_2^{2+} in 1 M $HClO_4$ (no exchange) displays a sharpening of the uranyl resonance line upon warming with $\Delta\nu_{1/2} = 14.0$ and 5.1 Hz at 273 and 323 K, respectively. In contrast, ^{17}O NMR spectra of UO_2^{2+} in 3.5 M (TMA)OH reveal a clear line broadening upon raising the temperature from 25 to 94 °C, as shown in the inset to Figure 7a. This spectral behavior is indicative of a ligand exchange process which is slow on the NMR time scale.[43] The other resonance observed in the ^{17}O NMR spectrum at $\delta = 10$ ppm sharpens upon warming. This resonance is assigned to the free and bound OH^- ligands, which are in fast equilibrium between themselves and the solvent, H_2O.

A standard line-broadening analysis was performed based on eq 4, where the width at half-height is composed of two parts, the natural line width in the absence of exchange, $1/T^\circ_2$, and the line broadening due to exchange, $1/T_2^{ex}$.[44] The natural line width (eq 5, where K = constant) is dependent on the temperature, T, and viscosity, η, of solution.[45] The solution viscosities were assumed to have a temperature dependence similar to that of H_2O (eq 6).[46] The value of $1/T_2^{ex}$ is equivalent to a first-order rate constant for the exchange process and is therefore related to the entropy and enthalpy of activation as shown in eq 7.[43] The accumulation of eqs 4−7 leads to three

$$\pi W_{1/2} = 1/T^\circ_2 + 1/T_2^{ex} \quad (4)$$

$$1/T^\circ_2 = K\eta/T \quad (5)$$

$$\eta_{water} = 241.4 \exp[570.58/(T - 140)] \quad (6)$$

$$1/T_2^{ex} = k_{ex} = (kT/h)[\exp(\Delta S^{\ddagger}/R)][\exp(-\Delta H^{\ddagger}/RT)] \quad (7)$$

unknowns, which were fitted to the line-width data using a standard least squares procedure. Figure 7b shows the line width data and the least-squares fit. From this analysis, activation

(33) Gordon, G.; Taube, H. *J. Inorg. Nucl. Chem.* **1961**, *19*, 189.
(34) Bányai, I.; Glaser, J.; Micskei, K.; Tóth, I.; Zékány, L. *Inorg. Chem.* **1995**, *34*, 3785.
(35) Gaziev, S. A.; Gorshkov, N. A.; Mashirov, L. G.; Suglobov, D. N. *Radiokhimiya* **1984**, *26*, 316.
(36) Gaziev, S. A.; Gorshkov, N. G.; Mashirov, L. G.; Suglobov, D. N. *Dokl. Akad. Nauk SSSR* **1985**, *285*, 630.
(37) Gaziev, S. A.; Gorshkov, N. G.; Mashirov, L. G.; Suglobov, D. N. *Radiokhimiya* **1986**, *28*, 755.
(38) Gaziev, S. A.; Gorshkov, N. G.; Mashirov, L. G.; Suglobov, D. N. *Radiokhimiya* **1986**, *28*, 764.
(39) von Felton, H.; Wernli, B.; Gamsjäger, H.; Baertschi, P. *J. Chem. Soc., Dalton Trans.* **1978**, 496.

Table 4. ^{17}O NMR Line-Width and Kinetic Data Analyis for U(VI) in 3.5 M (TMA)OH

	$W_{1/2}$ (Hz)	
Temp (K)	measd	calcd
298	29.50	30.00
318	55.26	53.67
328	80.05	80.59
338	122.32	123.16
348	188.07	187.66
356	263.20	276.61
$1/T_1^{283K}$ (s^{-1})	71 ± 7	
$1/T°_2^{283K}$ (s^{-1})	77 ± 3	
$\Delta H^{\ddagger}$ (kcal/mol)	9.8 ± 0.3	
$\Delta S^{\ddagger}$ (cal/mol·K)	-18 ± 4	
k_{ex}^{283K} (s^{-1})	18 ± 6	

parameters of $\Delta H^{\ddagger} = 9.8 \pm 0.3$ kcal/mol and $\Delta S^{\ddagger} = -18 \pm 4$ cal/mol·K were determined, indicating a thermally accessible and slightly ordered transition state. These activation parameters are similar to $\Delta H^{\ddagger} = 11.1 \pm 0.7$ kcal/mol and $\Delta S^{\ddagger} = -7.4 \pm 3$ cal/mol·K reported for bulk oxo ligand exchange on Np(VII) under alkaline conditions.[42] Table 4 contains a listing of the measured and calculated line widths and parameters obtained from the least-squares analysis.

Oxo ligand exchange between $UO_2(OH)_n^{2-n}$ ($n = 4$ and/or 5) and the bulk solvent was also confirmed by Raman spectroscopy using ^{18}O-enriched samples. For ^{18}O-enriched samples it was necessary to avoid the NO_3^- counterion, which displays a Raman peak at 740 cm^{-1} (see Figure 3), through replacement with $UO_2Cl_2 \cdot nH_2O$ in the starting materials. The Raman spectrum of $UO_2Cl_2 \cdot nH_2O$ dissolved in 3.5 M (TMA)-OH revealed a ν_1 Raman mode at 784 cm^{-1}, essentially identical to that for the NO_3^--containing solutions and confirming the presence of the $UO_2(OH)_5^{3-}$ ion. If the 784 cm^{-1} feature were solely a dioxo stretching mode, enriching the oxo ligands with 98% ^{18}O should produce a shift (6%) in the band to lower frequency, equivalent to the square root of the ratio of the atomic masses, i.e., $(16/18)^{0.5}$. Uranyl chloride was dissolved into a 3.5 M (TMA)OH solution prepared from 98% ^{18}O-enriched H_2O. The Raman spectrum showed only a single uranyl stretch around 752 cm^{-1}, which is only slightly higher than the 6% shift expected from the isotope mass effect on an isolated $[O{=}U{=}O]^{2+}$ moiety. The small difference is attributed to the system not being a pure isolated triatomic linear oscillator. The reversibility of oxo exchange was probed by drying the sample to remove $H_2{}^{18}O$, and the residue was subsequently redissolved in $H_2{}^{16}O$ to give an alkaline (TMA)OH solution of the same volume. The Raman spectrum of the redissolved residue showed the reappearance of the 784 cm^{-1} Raman band and a concomitant reduction of the 752 cm^{-1} band, suggesting a conversion of $U^{18}O_2(OH)_5^{3-}$ to $U^{16}O_2(OH)_5^{3-}$. A difference plot of the ^{18}O- and ^{16}O-labeled Raman spectra clearly indicates the presence of the two different vibrational modes (see Figure 3 inset).

Concluding Remarks

The pervasive tendency toward precipitation of insoluble uranate salts from highly alkaline solution has inhibited solution speciation studies aimed at determination of the identity and physicochemical properties of the limiting hydroxide complexes of the uranyl(VI) ion. We have shown that monomeric uranyl hydroxides, $UO_2(OH)_4^{2-}$ and $UO_2(OH)_5^{3-}$, can be stabilized from uranate formation using the Me_4N^+ (TMA^+) cation, thereby allowing for a full characterization under highly alkaline conditions. TMA^+ seems to be unique in this regard, as larger or smaller ammonium ions were unsuccessful at preventing precipitation.

The low-temperature emission and excitation spectral data clearly suggest that uranium(VI) in 0.75−2.5 M (TMA)OH exists as an equilibrium mixture of species, and the room-temperature absorption spectral data suggest that $UO_2(OH)_5^{3-}$ is the dominant solution species, especially at 3.5 M OH^-, the conditions of further study. The emission intensity data and the absorption data show that the concentration of $UO_2(OH)_5^{3-}$ (species A) increases relative to that of the other uranyl species, $UO_2(OH)_4^{2-}$ (B), as the hydroxide concentration increases. The Raman data and the vibronic data from the emission spectra both indicate the existence of a uranyl hydroxide species in these solutions with a totally symmetric stretching energy of ca. 786 cm^{-1}, and the Raman data indicate that this is the only detectable uranyl species in room-temperature solution (3.5 M OH^-). The EXAFS data for room-temperature solutions of UO_2^{2+} at similar (TMA)OH concentrations indicate that the average equatorial coordination number is ca. 5. In total, these spectral data indicate that the dominant uranyl species in (TMA)OH solution is the uranyl pentahydroxide $UO_2(OH)_5^{3-}$, but there is a small amount of another uranyl hydroxide species with fewer equatorial hydroxides (based on the emission intensity change versus hydroxide concentration). Given the solid state structural data presented here, it seems most probable that this other solution uranyl species is the tetrahydroxide, $UO_2(OH)_4^{2-}$.

The $UO_2(OH)_n^{2-n}$ ($n = 4, 5$) complexes display some unique structural and physicochemical properties. Both EXAFS and X-ray diffraction analyses reveal long axial U═O bonds (1.80−1.83 Å) and short equatorial U−OH bonds (2.21−2.26 Å). The lengthening and weakening of the U═O bond is confirmed by the low Raman frequency for the symmetrical O═U═O stretch, which at 786 cm^{-1} is the smallest reported value for any U(VI) complex, a shift of 84 cm^{-1} from the aquo ion value of 870 cm^{-1}.[27] The lengthening and weakening of the U═O bond may be partially explained by the strong σ-donating ability of the equatorial OH^- ligands. However, OH^- ligands are also strong π-donors, and multiple π-donor ligands coordinating to a single metal center (π-loading) can increase the stabilization of high-valent metals and generate a competition between oxo and hydroxo ligands for the same set of metal orbitals.[47] Although the exact nature of the electronic structure and bonding in uranyl systems is still under much debate,[48,49] there is general agreement that uranium 6d orbitals are involved in π-bonding in the O═U═O moiety. As a simple model, consider that, under D_{4h} symmetry, the 6d orbitals involved in axial U═O π-bonding have e_g symmetry. Of the O p−π lone pair orbitals on the four equatorial hydroxides, there is also one e_g representation, and competition between oxo and hydroxo ligands for use of the

(40) Roodt, A.; Leipoldt, J. G.; Helm, L.; Merbach, A. E. *Inorg. Chem.* **1994**, *33*, 140.
(41) Roodt, A.; Leipoldt, J. G.; Helm, L.; Abou, H. A.; Merbach, A. E. *Inorg. Chem.* **1995**, *34*, 560.
(42) Appelman, E. H.; Kostka, A. G.; Sullivan, J. C. *Inorg. Chem.* **1988**, *27*, 2002.
(43) Wilkins, R. G. *Kinetics and Mechanism of Reactions of Transition Metal Complexes*, 2nd ed.; VCH Publishers: New York, 1991.
(44) Johnson, C. S. In *Advances in Magnetic Resonance*; Waugh, J. S., Ed.; Academic: New York, 1965; Vol. 1, p 33.
(45) Klemperer, W. G. *Angew. Chem., Int. Ed. Engl.* **1978**, *17*, 246.
(46) Touloukian, Y. S.; Saxena, S. C.; Hestermans, P. *Thermophysical Properties of Matter*; IFI/Plenum: New York, 1975; Vol. 11.
(47) Nugent, W. A.; Mayer, J. M. *Metal-Ligand Multiple Bonds: the Chemistry of Transition Metal Complexes Containing Oxo, Nitrido, Alkylidene, or Alkylidyne Ligands*; Wiley: New York, 1988.
(48) Denning, R. G. *Struct. Bonding (Berlin)* **1992**, *79*, 215.
(49) Pepper, M.; Bursten, B. E. *Chem. Rev.* **1991**, *91*, 719.

uranium 6d e_g orbitals could be one rationalization for the weakening and lengthening of the U═O bond in $UO_2(OH)_4^{2-}$. Similar arguments can be made for $UO_2(OH)_5^{3-}$ under D_{5h} symmetry. In this regard, Schreckenbach et al. recently reported an extensive computational study of $UO_2(OH)_4^{2-}$ employing relativistic density functional theory which lends more quantitative support to the qualitative arguments presented here.[50] Furthermore, $UO_2(OH)_n^{2-n}$ ($n = 4, 5$) are examples of uranyl complexes with very weak room-temperature luminescence. Multiple bonding character in the equatorial plane, as well as OH^- acceptor vibrational modes, which can serve to quench the luminescence,[29,51,52] would correlate well with the low luminescence quantum yield.

It is also possible that the weakening and lengthening of the U═O bond (and concomitant U−OH multiple bond character) is related to the unusually facile oxo ligand exchange demonstrated by ^{17}O NMR and a combination of ^{16}O and ^{18}O Raman spectroscopy. The uranyl ion shows no chemical exchange under acidic and near-neutral aqueous solution conditions in the presence of common σ-donor ligands such as H_2O, Cl^-, NO_3^-, CO_3^{2-}, etc. However, with OH^- ligands capable of π-donation, a fairly rapid oxo ligand exchange process has been demonstrated. From the data amassed, one can propose either a direct (scheme A) or a water-assisted (scheme B) proton transfer between oxo and hydroxo ligands which may or may not be concerted. The hydroxide ions then exchange rapidly with the solvent as seen by a single, time average chemical shift for H_2O/OH^-. The activation parameters reported here are comparable in magnitude to the other examples of water-assisted oxo ligand exchange (scheme B) seen in alkaline solution and can be compared to $\Delta H^{\ddagger} = 15.0 \pm 0.6$ kcal/mol and $\Delta S^{\ddagger} = -10.4 \pm 2$ cal/mol·K determined for MoO_4^{2-},[39] which has been described as solvent-assisted oxygen dissociation where association between H_2O and MoO_4^{2-} plays an important role. To test these hypotheses will require finding a solvent other than water, where one can systematically vary the concentrations of water, hydroxide, etc. Additional studies to determine the detailed mechanism of chemical exchange, to determine the electronic structure and bonding, and to prepare the transuranic analogues are currently in progress.

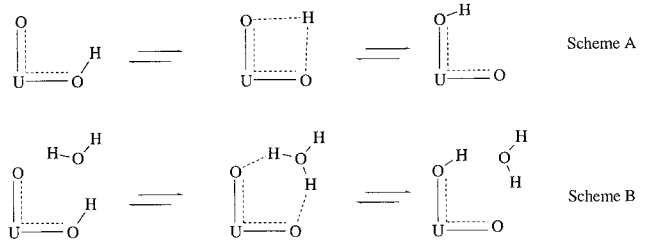

Experimental Section

General Considerations. All operations were carried out inside fume hoods or negative pressure gloveboxes designed for containment of radioactive materials. Standard radiochemical procedures were used throughout. $UO_2(NO_3)_2{\cdot}6H_2O$, $UO_2Cl_2{\cdot}nH_2O$, $Bu_4N(OH)$, NH_4OH, $Co(NH_3)_6Cl_3$, NaOH (Aldrich), and $Me_4N(OH)$ (Fisher) were all used as received. $UO_2(ClO_4)_2{\cdot}6H_2O$ was recrystallized three times from perchloric acid. ^{17}O-Enriched H_2O (20%) and ^{18}O-enriched H_2O (98%) were obtained from Los Alamos National Laboratory stock and used without further purificaton. Solution electronic absorption spectra were recorded on a double-beam Cary 5 UV−vis−near-IR spectrophotometer using matched 0.2 cm quartz cells or in a Perkin-Elmer Lambda 19 spectrophotometer with samples sealed in 1 cm quartz cuvettes. Continuous-wave (CW) and time-resolved (TR) luminescence data (emission and excitation spectra and emission decay curves) were obtained on a SPEX Industries Fluorolog System consisting of a Model 1681 single-stage 0.22 m excitation monochromator and a Model 1680 two-stage 0.22 m emission monochromator. CW spectra were obtained using the output from a high-intensity Xe arc lamp, and TR data were collected using a Model 1934D phosphorimeter attachment with a flash lamp excitation source. Most luminescence data were obtained at liquid-nitrogen temperature using a simple insertion dewar and front-face collection optics. Luminescence samples were contained in thick-walled borosilicate glass NMR tubes. Samples were not degassed prior to investigation. The emission and excitation data reported here have not been corrected for monochromator or detector response. Small variations in sample positioning with respect to the excitation source and the collection optics and mild fogging of the front face of the optical window on the dewar led to noticeable but uncorrectable variations in emission intensity. Thus, absolute intensity comparisons from one sample to the next are not possible. To extract vibrational data from the vibronically resolved emission spectra, the spectra were first transformed to the energy (cm^{-1}) domain. Unconstrained spectral fits with Gaussian or Voigt functions were used to get accurate peak locations. NMR spectra were recorded on a Bruker AMX500 spectrometer with a 5 mm broadband probe operating at 67.8 (^{17}O) MHz with a ^2H field-frequency lock; the peak positions are reported with positive shifts downfield of external H_2O set at $\delta = 0.0$ ppm. The temperature was controlled with a Bruker variable-temperature controller and was stable to within ±1 K. The temperature was determined by measurement of the ^1H NMR spectra of ethylene glycol (295−350 K). For each ^{17}O NMR sample, the solution was transferred to a 4 mm o.d. Teflon FEP NMR tube insert (Wilmad), which was subsequently heat sealed using a small soldering gun. The Teflon insert was then transferred to a standard 5 mm o.d. glass NMR tube. The 4% enriched UO_2^{2+} in 1 M $HClO_4$ was prepared by standard electrochemical methods[18,53] starting with $UO_2(NO_3)_2{\cdot}6H_2O$. The final concentration of uranium was determined by UV−vis spectroscopy using the 415 nm absorption feature ($\epsilon = 8\ M^{-1}\ cm^{-1}$). Raman vibrational spectra were obtained by exciting from an Ar^+ laser (Spectra Physics, Model 2025) using 457.9, 488.0, 496.5, or 514.5 nm lines. The laser power at the sample was ≈25 mW. The scattered light was dispersed and analyzed on a SPEX Model 1403 scanning double monochromator equipped with an 1800 groove/mm grating and a single-photon-counting detection system. The spectral slit width was maintained at 5 cm^{-1} resolution. Scan parameters were 1 cm^{-1} increments between points, integration for 2−3 s at each point, and at least 75−99 scans averaged for the final spectrum. The Raman samples were recorded in sealed 5 mm glass NMR tubes. Because of photodecomposition of the $[Co(NH_3)_6]_2[UO_2(OH)_4]_3{\cdot}H_2O$ solid using visible excitation, Raman spectra of the solid sample were recorded in the near-infrared through excitation with a Ti-sapphire CW laser (752 nm, Spectra Physics Model 3900S) and detection was accomplished through a CCD detector (Princeton Instruments). The Raman scattering was dispersed with a single-stage monochromator (diffraction gratings blazed at 1150 nm, 4 cm^{-1} resolution) after being prefiltered through an interference filter designed to remove Rayleigh scattered laser light.

Synthesis of $[Co(NH_3)_6]_2[UO_2(OH)_4]_3{\cdot}H_2O$. To a stirring solution of $UO_2(NO_3)_2{\cdot}6H_2O$ (0.012 M) in 3.5 M (TMA)OH was added a dilute solution of $Co(NH_3)_6Cl_3$ (0.01 M), and the reaction mixture was cooled to 5 °C. Small orange crystals of $[Co(NH_3)_6]_2[UO_2(OH)_4]_3{\cdot}H_2O$ were deposited after 12 h in essentially quantitative crystallized yield. These crystals are slightly soluble in 3.5 M (TMA)OH and MeOH solutions.

Solution Preparations. Electronic Spectroscopy. (A) A 0.114 M U(VI) solution in 3.5 M (TMA)OH was prepared by dissolving $UO_2(NO_3)_2{\cdot}6H_2O$ (86 mg, 0.15 mmol) in 1.5 mL of 3.5 M (TMA)OH. The yellow solution was centrifuged (5 min at 5000 rpm) with the resulting clear solution being transferred to 0.2 cm quartz cells. The visible

(50) Schreckenbach, G.; Hay, P. J.; Martin, R. L. *Inorg. Chem.* **1998**, *37*, 4442.
(51) Moulin, C.; Decambox, P.; Moulin, V.; Decaillon, J. G. *Anal. Chem.* **1995**, *67*, 348.
(52) Horrocks, W. D.; Sudnick, D. R. *J. Am. Chem. Soc.* **1979**, *101*, 334.
(53) Hobart, D. E.; Samhoun, K.; Peterson, J. R. *Radiochim. Acta* **1982**, *31*, 139.

spectrum from 350 to 600 nm was monitored and showed four peaks in the range 380−430 nm with $\epsilon_{400.2} = 33.2\ M^{-1}\ cm^{-1}$. **(B)** For the titration study, U(VI) samples were prepared from 13 mL of a uranyl stock solution (2 M $UO_2(NO_3)_2 \cdot 6H_2O$ in 1M $HClO_4$) and 687 mL of 3.5, 1.75, 0.85, 0.43, and 0.05 M (TMA)OH solution, respectively. After preparation, each clear yellow solution was transferred into a 0.2 cm cell and the visible spectrum recorded.

EXAFS Data Acquisition and Analysis. $UO_2(NO_3)_2 \cdot 6H_2O$ (22 mg, 0.044 mmol) was dissolved in 0.450 mL of 3.5 M TMAOH. After centrifuging for 10 min at 6000 rpm, the yellow solution was transferred to a 4 mm o.d. Teflon tube and heat sealed. The filled Teflon tube was mounted to the interior of an EXAFS sample holder, which was then subsequently doubly contained with Kapton film. **Warning:** (TMA)OH is corrosive and will slowly dissolve Kapton. Uranium L_{III} edge X-ray absorption spectra were collected at the Stanford Synchrotron Radiation Laboratory on wiggler beamline 4-2 (unfocused) with an electron beam energy of 3.0 GeV and beam currents between 60 and 100 mA. A Si (220) double-crystal monochromator was used. Rejection of higher harmonic content in the X-ray beam was achieved by employing a flat Rh-coated quartz mirror tuned at a critical angle for the rejection of photons having energies above 24 000 eV. Having rejected greater than 95% of the higher order harmonics with the mirror, the monochromator was operated fully tuned with respect to θ, the orientation between the two crystals. Spectra were collected simultaneously both in transmission mode using N_2-filled ion chamber detectors and in fluorescence mode using a 13-element Ge detector (EG&G ORTEC). For the Ge detector, the count rate was controlled by adjusting the hutch entrance slits or by changing the sample−detector distance. Data reduction and analysis were performed using techniques described elsewhere.[54] The summed data for each detector (transmission or fluorescence) were then inspected, and only those channels that gave high-quality signal-to-noise ratios were included in the final weighted average. Three EXAFS scans were collected on the solution at ambient temperature (ca. 25 °C). The spectra were energy calibrated by measuring the spectrum of a Zr foil and defining the first inflection point at the Zr K-edge as 17 999.35 eV. The data were manipulated and analyzed using either WinXAS 97[55] or in-house data analysis programs. The data were normalized by offsetting the spectrum so that the value of a second-order polynomial fit through the pre-edge was 0 at E_0, and the value of the second-order polynomial through the EXAFS region was unity. A cubic spline function was used to fit the background over the EXAFS region, which extended out to $k = 11.7\ Å^{-1}$. Fourier transforms of the k^3-weighted data were calculated over the range $k = 3.00-11.70\ Å^{-1}$. Theoretical phases and amplitudes were derived from the program FEFF7[19,20] to fit the contributions from the O neighbors. The parameters refined in the fit were ΔE_0, the photoelectron energy threshold; R_i, the distance from U to atom i; n_i, the number of i atoms; and σ_i, the DW term for atom i. The quality of the fit was determined by the residium between the fit and k-space data.

Preparation of U(VI) Samples in 3.5 M TMAOH for Raman Analysis. (A) Uranyl Nitrate. A portion of the solution (300 μL) prepared for part A of the visible experiment was transferred to a sample tube and the Raman spectrum recorded. Raman shift (cm^{-1}): 786. **(B) Uranyl Chloride.** $UO_2Cl_2 \cdot H_2O$ (0.052 g, 0.14 mmol) was dissolved in 1.0 mL of 3.5 M (TMA)OH, giving a yellow-colored solution. After centrifugation (10 min at 5000 rpm), the clear solution was transferred to a sample tube for analysis. Raman shift (cm^{-1}): 784.

Raman ^{18}O-Labeling Study. $UO_2Cl_2 \cdot H_2O$ (32 mg, 0.09 mmol) was dissolved in 0.5 mL of 98% ^{18}O-enriched 3.5 M (TMA)OH, resulting in a yellow-colored solution. After centrifugation (10 min at 5000 rpm), the clear solution was transferred to a sample tube for Raman analysis. Raman shift (cm^{-1}): 752. After the Raman spectrum was obtained, the solution was dried by warming (80 °C) under reduced pressure. The resulting residue was redissolved in nonenriched H_2O and the Raman spectrum collected. Raman shift (cm^{-1}): 784.

^{17}O NMR Samples. The NMR samples were prepared using a 4% enriched uranyl stock solution (1.22 M UO_2^{2+} in 1 M $HClO_4$). To obtain a highly enriched solution of approximately 0.1 M UO_2^{2+} and 3.5 M (TMA)OH, 50 μL (0.061 mmol) of the uranyl stock solution was added to D_2O (10 μL), 20.4% enriched $H_2{}^{17}O$ (390 μL), and (TMA)OH·$5H_2O$ (341 mg, 1.71 mmol). The low-enrichment samples were prepared in a similar fashion. An aliquot (50 μL, 0.061 mmol) of the uranyl stock solution was added to D_2O (10 μL), nonenriched H_2O (390 mL), and (TMA)OH·$5H_2O$ (324 mg, 1.62 mmol), resulting in a final solution containing 0.1 M UO_2^{2+}. A 0.03 M UO_2^{2+} solution was also prepared by adding 10 μL of the uranyl stock solution to unenriched D_2O (800 μL) and (TMA)OH·$5H_2O$ (748 mg, 3.74 μmol). ^{17}O NMR (H_2O, 298 K, δ): 1117 ($W_{1/2} = 29.50\ s^{-1}$, $T_1 = 14 \pm 2$ ms).

X-ray Crystallography. Yellow platelike crystals of $[Co(NH_3)_6]_2[UO_2(OH)_4]_3 \cdot H_2O$ were prepared from a solution containing 0.010 M $[Co(NH_3)_6]Cl_3$ and 0.012M $UO_2(NO_3)_2 \cdot 6H_2O$ in 3.5 M (TMA)OH, which was subsequently centrifuged and cooled to 5 °C for 2 days. A pale yellow plate with dimensions 0.30 × 0.25 × 0.10 was mounted on a fiber and transferred to the goniometer of a Siemens SMART diffractometer equipped with a CCD area detector. The crystal was cooled to −100 °C during data collection by using a stream of cold nitrogen gas. The space group was determined to be either the centric $C2/c$ or acentric Cc from the systematic absences. The subsequent solution and successful refinement of the structure was carried out in the centric space group $C2/c$. A summary of the data collection parameters is given in Table 1.

The N-bound hydrogen atoms were included as a rigid group (maximizing the electron density at the three calculated H atom positions) with rotational freedom at the bonded nitrogen atom ($B = 1.2U_{eqv}$ (N)). The hydroxide hydrogen atom positions were calculated by idealizing the U−O−H angle at a tetrahedral value with a torsion angle chosen to maximize the electron density. These hydrogen atoms were included in a riding model with $B = 1.2U_{eqv}$ (O). Each of these hydrogen atoms is located between the bonded O atom and a hydrogen bond acceptor.

The aquo hydrogen atoms were located from a difference Fourier map. These positions are less accurate; however, electron density was found which indicated directionality toward hydrogen bond acceptors. One of the two unique positions found resided on a 2-fold axis, while the second with roughly half the peak height of the former was in a general position and was included at half-occupancy. These hydrogen atoms were allowed to ride on O(11) with $B = 1.2U_{eqv}$ (O(11)). Refinement of non-hydrogen atoms was carried out with anisotropic temperature factors.

Acknowledgment. We wish to thank Drs. N. M. Edelstein, P. J. Hay, R. L. Martin, M. P. Neu, T. W. Newton, W. Runde, and G. Schreckenbach for helpful discussions. This research was jointly sponsored by the offices of Energy Research and Environmental Management and administered by the office of Basic Energy Sciences, Division of Chemical Sciences, U.S. Department of Energy, under Contract W-7405-eng-36 with the University of California. XAFS experiments were performed at the Stanford Synchrotron Radiation Laboratory, which is supported by the U.S. DOE Office of Basic Energy Sciences.

Supporting Information Available: An X-ray crystallographic file, in CIF format, for the structure determination of $[Co(NH_3)_6]_2[UO_2(OH)_4]_3 \cdot H_2O$ is available. This material is available free of charge via the Internet at http://pubs.acs.org.

IC981137H

(54) Prins, R.; Koningsberger, D. C. *X-ray Absorption: Principles, Applications, Techniques for EXAFS, SEXAFS, and XANES*; Wiley: New York, 1988.
(55) Ressler, T. *J. Phys. IV* **1997**, *7*, C2.